International Journal of Thermal Sciences 102 (2016) 263–273

Contents lists available at ScienceDirect

International Journal of Thermal Sciences

journal homepage: www.elsevier.com/locate/ijts

Non-Fourier heat conduction in a sandwich panel with a cracked foam core

J.W. Fu [a, 1], A.H. Akbarzadeh [b, c, *, 1], Z.T. Chen [d], L.F. Qian [a], D. Pasini [c, **]

[a] Department of Mechanical Engineering, Nanjing University of Science and Technology, Nanjing 210094, China
[b] Department of Bioresource Engineering, McGill University, Ste-Anne-de-Bellevue, Island of Montreal, QC H9X 3V9, Canada
[c] Department of Mechanical Engineering, McGill University, Montreal, QC H3A 0C3, Canada
[d] Department of Mechanical Engineering, University of Alberta, Edmonton, AB T6G 2G8, Canada

ARTICLE INFO

Article history:
Received 9 April 2015
Received in revised form
21 November 2015
Accepted 27 November 2015
Available online xxx

Keywords:
Foam core
Heat flux intensity factor
Non-Fourier heat conduction
Porous material
Sandwich panel
Thermally insulated crack

ABSTRACT

Crack formation in cellular solids is often triggered by the presence of flaws caused by the manufacturing process that is used to build them. In thermal management applications, an imperfection embedded in the core of a sandwich panel might have a detrimental thermal impact that is often challenging to predict. This paper focuses on a theoretical study of non-Fourier heat conduction in a sandwich panel with a cracked foam core. With the aim of exploring the thermal response of a panel with porous core and skins made of a single material, we examine the role of crack position, relative density of the foam core, and other geometric parameters of the panel. Based on the assumption that the crack in the core is thermally insulated, i.e. no heat flux can pass through, we obtain the temperature distribution and heat flux intensity factor in the time domain via Fourier and Laplace transforms. The results are visualized in maps that show the influence of the size of the skin relative to that of the foam core and the crack location as well as the antagonist impact that the relative density of the foam core has on the maximum temperature and heat flux. The method presented here can be used to tailor the thermal response of sandwich panels.

1. Introduction

Sandwich panels consist of two stiff and strong skins, or faces, bonded to a core [1]. While the former are typically metal or polymer/fiber-reinforce composites, the core has generally a low-density cellular architecture, such as that in metallic honeycombs, polyurethane foams, and other porous materials. The function of the core is to not only increase the bending stiffness of the panel and its resistance to buckling loads [1,2], but also satisfy multi-functional requirements, such as fluid permeability, energy absorption, and acoustic damping among others [3,4]. Low weight, structural efficiency, and multifunctionality, are desirable characteristics often sought after in aircrafts, automobiles, ships, and sport equipment. Usually, the cellular architecture of the core can be either random, such as in foams, or periodic, such as in corrugated (prismatic) metals and textile/truss cores [4], but it might be also a mix of them. In general, what controls the multifunctional response of a sandwich panel is the properties of the skin and the core. The thickness of the former, besides its material attributes, is a critical design parameter, whereas the relative density of the latter, i.e. the core, together with cell topology and nodal connectivity, governs the thermal, acoustic, and other responses of the sandwich panel.

Due to the increasing use of cellular materials in multifunctional applications, the study of their multiphysics has been the object of intense research. A wealth of studies is available in the literature, each dealing with either the theoretical and/or experimental aspects. On the prediction side, for instance, several homogenization schemes applied to cellular materials have been used to predict heat conduction and mass transport [5–8], electromagnetic permeability [9], as well as their mechanical responses [10–15]. On the testing side, the mechanical [16,17], thermal [18,19], and thermomechanical [20–22] responses of a sandwich panel with either a lattice or foam architecture have been measured for the use in load-bearing, biomedical, and thermal management applications.

In structural applications, the presence of a crack, either within the core or at the interface with the skins, can utterly drop the

* Corresponding author. Department of Bioresource Engineering, McGill University, Ste-Anne-de-Bellevue, Island of Montreal, QC H9X 3V9, Canada. Tel.: +1 514 398 7680; fax: +1 514 398 7990.
** Corresponding author.
E-mail addresses: hamid.akbarzadeh@mcgill.ca (A.H. Akbarzadeh), damiano.pasini@mcgill.ca (D. Pasini).
[1] These authors contributed equally to this work.

http://dx.doi.org/10.1016/j.ijthermalsci.2015.11.011
1290-0729/

strength of the panel [23]. The magnitude of this reduction, as well as its associated evolution of fracture, have been studied by using standard concepts of continuum and fracture mechanics [24,25]. Whereas some studies have mainly examined the nucleation and propagation of a crack in a cellular material [9,26], others have focused on the cellular core in a sandwich panel, in particular its failure modes, such as the formation of an inter-layer crack and skin delamination [17].

In thermal management applications, a crack that forms in a sandwich core causes overheating its vicinity. The physics of this phenomenon poses some challenges for both the theory and experiments that are required to understand it [27–29]. First investigations back to 1965 examined a solid material containing a crack, where the singularity of the heat flux was obtained in steady state for an infinite medium with collinear cracks [30]. To quantify thermal energy accumulated around a macro-crack tip, Tzou [31,32] first introduced the intensity factor of the temperature gradient and then analyzed the effect of the thermal properties on the singularity exponent of the temperature gradient. More recently, the influence of an arbitrarily oriented crack on the heat conduction of a functionally graded (FG) medium has been elucidated and the discontinuity of the heat flux has been obtained via the heat flux intensity factor (HFIF) [33]. Similar to the concept of the stress intensity factor measuring the stress concentration in the vicinity of a crack tip, HFIF represents the intensification scale of the heat flux at the crack tip [34]. A larger value of HFIF implies a higher heat flux and a severer thermal condition around the crack tip. While the aforementioned studies pertain to a crack in a solid material, transient heat conduction analysis of a cellular material containing a crack is at its infancy and limited to Fourier heat conduction [35,36].

Fourier heat conduction is the conventional approach that has been extensively used to study heat conduction in crack problems. Although well established, one limitation of this theory is its accuracy, which is deficient for very low temperature and short-pulse thermal heating in micro temporal/spatial scale [37,38]. As a result, non-Fourier heat conduction schemes have been proposed, among which the simplest is that of Cattaneo–Vernotte (C–V) [39,40]. Another refinement, introduced by Tzou [41] to better describe heat conduction in a transient case, resorts to a dual-phase-lag (DPL) that accounts for the microscale temporal and spatial effects of the heat transport. The DPL model has been used to investigate heat conduction in layered composites [42], interface bonding of dissimilar materials [43], biological tissues [44], and FG materials [45–48]. Recently, non-Fourier theories have been also applied to solid media containing a crack, and to study the transient heat conduction in a cracked half-space [49], a bilayered composite with a penny-shaped interfacial crack [50], as well as a cylinder with an embedded/edge circumferential crack [51]. It has been observed that the phase-lags of heat flux and temperature gradient have a significant impact on the intensity factors of a cracked medium. Furthermore, DPL theory applied to a sandwich panel subjected to a thermal shock has the potential to capture the thermal wave propagation and the overshooting of the transient temperature induced by the thermal impact. Another advantage of using the DPL theory is that microstructural interactions occurring during the heat transport process and fast transient phenomena of thermal waves can be studied via the phase-lag of the heat flux. Despite these pros, no work exists in the current literature that uses non-Fourier heat conduction to understand the transient thermal response of a sandwich panel with a cracked core.

This paper aims at studying the disturbed temperature field of a sandwich panel, containing an insulated crack in its core that is made of foam. Both skins and core are assumed to be made of a single material, and the overall panel assumed to be rigid with no deformation occurring under transient thermal loadings. We use a DPL heat conduction model (Section 2) with the effective thermal properties of foams (Section 3) for thermal analysis. In Section 4, the two-dimensional temperature field is obtained in Laplace domain by Fourier transform and by solving singular integral equations. We also introduce HFIF to recognize the singularity of the heat flux field at the crack tip. The role of phase-lags, relative density, skin thickness, and crack position is examined in Section 5 with respect to the transient temperature field and HFIF, and the results are illustrated in the form of design charts [52–54].

2. Problem definition

We examine a sandwich panel with a foam core containing a thermally insulated crack, assumed here as a gap of length $2c$ (Fig. 1) [55]. The sandwich consists of: (1) an upper skin with thickness $h_3 - h_1$, (2) foam core of thickness $h_1 + h_2$, and (3) lower skin of thickness $h_4 - h_2$. The material properties of both skin and core do not change. The sandwich panel is initially at temperature T_∞, before applying a sudden temperature rise at the top, T_a, and the bottom, T_b, of the skins. Temperature rises occur via a Heaviside or step function $H(t)$, which is zero for negative values of t and is unity for non-negative values of t. In this investigation, since the solid skins and foam core are made of one material, there is a unique coefficient of thermal expansion, which does not change for the relative density range of the foam core. The result is that no residual stresses can develop at the interface between the skins and foam core with a perfect bond.

The DPL model for heat conduction can be described as:

$$\mathbf{q}(\mathbf{r}, t + \tau_q) = -k\nabla T(\mathbf{r}, t + \tau_T) \tag{1}$$

where $\mathbf{q}$, $\mathbf{r}$, t, k, and T are the heat flux vector, position vector, time, thermal conductivity, and temperature, respectively; ∇ represents the gradient operator and τ_q and τ_T are phase-lags of heat flux and temperature gradient, respectively. We use the Taylor series expansion (Eq. (1)) up to the second-order for τ_q, and up to the first-order for τ_T, which leads to the wave-like DPL model [45]

$$\left(1 + \tau_q\frac{\partial}{\partial t} + \frac{1}{2}\tau_q^2\frac{\partial^2}{\partial t^2}\right)\mathbf{q} = -k\left(1 + \tau_T\frac{\partial}{\partial t}\right)\nabla T \tag{2}$$

The energy conservation equation in the absence of internal heat generation is written as

$$-\nabla\cdot\mathbf{q} = \rho c_V\frac{\partial T}{\partial t} \tag{3}$$

where ρ and c_V are, respectively, mass density and specific heat capacity. Eliminating $\mathbf{q}$ in Eqs. (2) and (3) leads to the following hyperbolic differential equation:

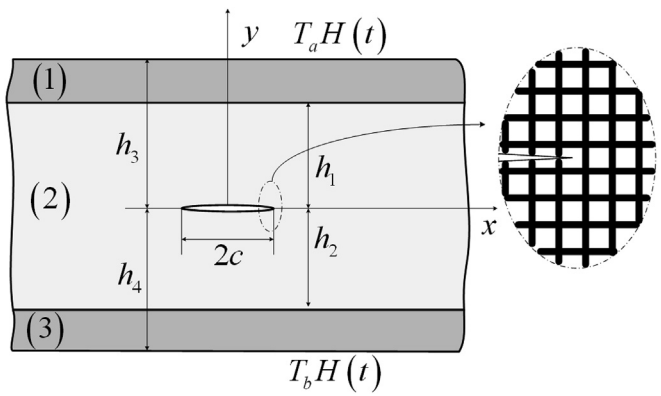

Fig. 1. A mono-dimensional sandwich panel with a cracked foam core.

$$\left(1+\tau_q\frac{\partial}{\partial t}+\frac{1}{2}\tau_q^2\frac{\partial^2}{\partial t^2}\right)\frac{\partial T}{\partial t}=d\left(1+\tau_T\frac{\partial}{\partial t}\right)\nabla^2 T \tag{4}$$

where $d=k/(\rho c_V)$ is the thermal diffusivity.

3. Effective thermal properties of the sandwich core

The sandwich core, examined in this work, is a foam with a random arrangement of cells [56,57]. To avoid a detailed microscale analysis of the foam architecture, we use its effective thermal properties obtained via homogenization [12,14,58]. If we assume local thermal equilibrium and neglect radiative effects, viscous dissipation, and work done by pressure changes, the effective heat capacity of a foam (in the unit of J/(m^3 K)) [59,60] can be written as:

$$\overline{\rho}\overline{c}_V=(\rho_s c_{Vs})\rho_r+(\rho_g c_{Vg})(1-\rho_r) \tag{5}$$

where the subscripts "s" and "g" refer to the material properties of solid and gas; overbar denotes the effective material properties. The relative density ρ_r is defined as:

$$\rho_r=\frac{\overline{\rho}}{\rho_s} \tag{6}$$

where ρ_s is the material density of the solid of which the foam is made [61]. If the heat convection of the gas in the foam is neglected, its thermal conductivity can be written as [57]

$$\overline{k}=\frac{1}{3}\left(\rho_r+2\rho_r^{3/2}\right)k_s+(1-\rho_r)k_g \tag{7}$$

If the heat capacity and thermal conductivity of gas are assumed equal to those of dry air, then $\rho_g c_{Vg}=1.006\times10^3$ J/(m^3 K) and $k_g=0.025$ W/(m K) [5]. Equations (5) and (7) are used in the following sections for thermal analysis, where overbar is omitted for simplicity in the rest of formulations. In addition, we assume the phase-lags of the cellular medium equal to those of the solid material.

4. Methodology

For a two-dimensional temperature field, the governing equations can be written in Cartesian coordinates using Eq. (4):

$$\left(1+\tau_q\frac{\partial}{\partial t}+\frac{1}{2}\tau_q^2\frac{\partial^2}{\partial t^2}\right)\frac{\partial T^{(\alpha)}}{\partial t}=d^{(\alpha)}\left(1+\tau_T\frac{\partial}{\partial t}\right)\left(\frac{\partial^2}{\partial x^2}+\frac{\partial^2}{\partial y^2}\right)T^{(\alpha)}\quad(\alpha=1,2,3) \tag{8}$$

where the superscript "α" denotes the αth layer. The following non-dimensional parameters are here introduced:

$$t'=\frac{td^{(0)}}{c^2},\ \tau_q'=\frac{\tau_q d^{(0)}}{c^2},\ \tau_T'=\frac{\tau_T d^{(0)}}{c^2},\ x'=\frac{x}{c},\ y'=\frac{y}{c},\ h_j'=\frac{h_j}{c}\quad(j=1,2,3,4)$$
$$T^{(\alpha)'}=\frac{T^{(\alpha)}-T_\infty}{T_\infty},\ T_a'=\frac{T_a-T_\infty}{T_\infty},\ T_b'=\frac{T_b-T_\infty}{T_\infty},\ \mathbf{q}^{(\alpha)'}=\frac{\mathbf{q}^{(\alpha)}c}{k^{(0)}T_\infty} \tag{9}$$

where $d^{(0)}$ and $k^{(0)}$ are the thermal diffusivity and thermal conductivity of the constituent solid materials. Equation (8) can be rewritten as

$$\left(1+\tau_q'\frac{\partial}{\partial t'}+\frac{1}{2}\tau_q'^2\frac{\partial^2}{\partial t'^2}\right)\frac{\partial T^{(\alpha)\prime}}{\partial t'}=\frac{d^{(\alpha)}}{d^{(0)}}\left(1+\tau_T'\frac{\partial}{\partial t'}\right)\left(\frac{\partial^2}{\partial x'^2}+\frac{\partial^2}{\partial y'^2}\right)T^{(\alpha)\prime} \tag{10}$$

Considering zero initial conditions, the Laplace transform is applied to Eq. (10) [62]

$$\left(\frac{\partial^2}{\partial x'^2}+\frac{\partial^2}{\partial y'^2}\right)\widetilde{T}^{(\alpha)\prime}-\lambda^{(\alpha)}(s)\widetilde{T}^{(\alpha)\prime}=0 \tag{11}$$

where

$$\lambda^{(\alpha)}(s)=\frac{d^{(0)}}{d^{(\alpha)}}\cdot\frac{\left(1+\tau_q's+\frac{1}{2}\tau_q'^2s^2\right)s}{1+\tau_T's} \tag{12}$$

and s represents the Laplace variable.

By assuming thermally insulated crack surfaces and imperfectly conducting interfaces, non-dimensional boundary conditions can be expressed in the Laplace domain as

$$\widetilde{T}^{(1)\prime}(x',h_3',s)=T_a'/s \tag{13-1}$$

$$\widetilde{T}^{(3)\prime}(x',-h_4',s)=T_b'/s \tag{13-2}$$

$$X_1\widetilde{q}_y^{(1)\prime}(x',h_1',s)=\widetilde{T}^{(2)\prime}(x',h_1',s)-\widetilde{T}^{(1)\prime}(x',h_1',s) \tag{14-1}$$

$$\widetilde{q}_y^{(1)\prime}(x',h_1',s)=\widetilde{q}_y^{(2)\prime}(x',h_1',s) \tag{14-2}$$

$$X_2\widetilde{q}_y^{(3)\prime}(x',-h_2',s)=\widetilde{T}^{(3)\prime}(x',-h_2',s)-\widetilde{T}^{(2)\prime}(x',-h_2',s) \tag{14-3}$$

$$\widetilde{q}_y^{(2)\prime}(x',-h_2',s)=\widetilde{q}_y^{(3)\prime}(x',-h_2',s) \tag{14-4}$$

$$\widetilde{q}_y^{(2)\prime}\left(x',0^+,s\right)=\widetilde{q}_y^{(2)\prime}\left(x',0^-,s\right),\quad |x'|\geq 1 \tag{15}$$

$$\widetilde{q}_y^{(2)\prime}\left(x',0^+,s\right)=0,\quad |x'|<1 \tag{16-1}$$

$$\widetilde{T}^{(2)\prime}\left(x',0^+,s\right)=\widetilde{T}^{(2)\prime}\left(x',0^-,s\right),\quad |x'|\geq 1 \tag{16-2}$$

where $q_y^{(\alpha)}$ is the heat flux component in y-direction; the variables with tilde "~" indicate their counterparts in the Laplace domain; X_1 and X_2 are non-negative constants representing weak thermal interface between skins and core of the sandwich panel [60,63]. For the sake of brevity, however, perfect thermal interfaces are considered in this analysis ($X_1=X_2=0$). Considering Eq. (2), $\widetilde{q}_y^{(\alpha)\prime}$ is expressed in terms of temperature as follows:

$$\widetilde{q}_y^{(\alpha)\prime} = -\beta^{(\alpha)}(s)\frac{\partial \widetilde{T}^{(\alpha)\prime}}{\partial y'} \tag{17}$$

where

$$\beta^{(\alpha)}(s) = \frac{k^{(\alpha)}}{k^{(0)}}\cdot\frac{1+\tau_T' s}{1+\tau_q' s+\frac{1}{2}\tau_q'^2 s^2} \tag{18}$$

The governing equation (11) subjected to the boundary conditions (13)–(16) can be solved by decomposing the present problem into: (a) an undamaged sandwich panel with inhomogeneous thermal boundaries and (b) a cracked one with homogeneous boundary conditions [64,65]. The latter can be solved via Fourier transform. As a result by superposition, we obtain the temperature field in the Laplace domain:

$$\begin{aligned}\widetilde{T}^{(1)\prime}(x',y',s) = \frac{1}{2\pi}\int_{-\infty}^{\infty}&\left[D_1\exp\left(m^{(1)}y'\right)+D_2\exp\left(-m^{(1)}y'\right)\right]\\ &\times\exp(\mathrm{i}\xi x')\mathrm{d}\xi + C_1^{(1)}\exp\left(\sqrt{\lambda^{(1)}}y'\right)+C_2^{(1)}\\ &\times\exp\left(-\sqrt{\lambda^{(1)}}y'\right),\quad h_1'<y'\le h_3'\end{aligned} \tag{19-1}$$

$$\begin{aligned}\widetilde{T}^{(2)\prime}(x',y',s) = \frac{1}{2\pi}\int_{-\infty}^{\infty}&\left[D_3\exp\left(m^{(2)}y'\right)+D_4\exp\left(-m^{(2)}y'\right)\right]\\ &\times\exp(\mathrm{i}\xi x')\mathrm{d}\xi + C_1^{(2)}\exp\left(\sqrt{\lambda^{(2)}}y'\right)+C_2^{(2)}\\ &\times\exp\left(-\sqrt{\lambda^{(2)}}y'\right),\quad 0<y'\le h_1'\end{aligned} \tag{19-2}$$

$$\begin{aligned}\widetilde{T}^{(2)\prime}(x',y',s) = \frac{1}{2\pi}\int_{-\infty}^{\infty}&\left[D_5\exp\left(m^{(2)}y'\right)+D_6\right.\\ &\left.\times\exp\left(-m^{(2)}y'\right)\right]\exp(\mathrm{i}\xi x')\mathrm{d}\xi + C_1^{(2)}\\ &\times\exp\left(\sqrt{\lambda^{(2)}}y'\right)+C_2^{(2)}\exp\left(-\sqrt{\lambda^{(2)}}y'\right),\\ &-h_2'\le y'<0\end{aligned} \tag{19-3}$$

$$\begin{aligned}\widetilde{T}^{(3)\prime}(x',y',s) = \frac{1}{2\pi}\int_{-\infty}^{\infty}&\left[D_7\exp\left(m^{(3)}y'\right)+D_8\right.\\ &\left.\times\exp\left(-m^{(3)}y'\right)\right]\exp(\mathrm{i}\xi x')\mathrm{d}\xi + C_1^{(3)}\\ &\times\exp\left(\sqrt{\lambda^{(3)}}y'\right)+C_2^{(3)}\exp\left(-\sqrt{\lambda^{(3)}}y'\right),\\ &-h_4'\le y'<-h_2'\end{aligned} \tag{19-4}$$

where $m^{(\alpha)}=\sqrt{\xi^2+\lambda^{(\alpha)}}$. The unknown coefficients $C_1^{(\alpha)}$ and $C_2^{(\alpha)}$ are determined by solving the temperature field of a sandwich panel without crack:

$$\mathbf{EC}=\mathbf{A} \tag{20}$$

where

$$\mathbf{C}=\left[C_1^{(1)}\quad C_2^{(1)}\quad C_1^{(2)}\quad C_2^{(2)}\quad C_1^{(3)}\quad C_2^{(3)}\right]^{\mathrm{T}} \tag{21}$$

and **E** and **A** are, respectively, a 6 × 6 matrix and a 6 × 1 vector, whose non-zero elements are given in the Appendix.

Substituting Eqs. (19-1)–(19-4) into the homogeneous part of the boundary conditions (13)–(15) results in

$$D_1=-D_2\exp\left(-2m^{(1)}h_3'\right),\quad D_8=-D_7\exp\left(-2m^{(3)}h_4'\right) \tag{22-1}$$

$$D_3=\chi_1 D_2/2,\quad D_4=\chi_2 D_2/2,\quad D_5=\chi_3 D_7/2,\quad D_6=\chi_4 D_7/2 \tag{22-2}$$

$$D_7=\frac{\chi_1-\chi_2}{\chi_3-\chi_4}D_2 \tag{22-3}$$

with coefficients χ_j given in the Appendix. The unknown coefficient D_2 is obtained by applying the mixed boundary condition (Eq. (16)), and introducing the following unknown function:

$$\phi(x',s)=\frac{\partial}{\partial x'}\left[\widetilde{T}_2^{(2)\prime}\left(x',0^+,s\right)-\widetilde{T}_2^{(2)\prime}\left(x',0^-,s\right)\right] \tag{23}$$

Using Eqs. (16-2) and (23), one can obtain

$$\phi(x',s)=0,\quad |x'|\ge 1 \tag{24-1}$$

$$\int_{-1}^{1}\phi(x',s)\mathrm{d}x'=0,\quad |x'|<1 \tag{24-2}$$

Substituting Eqs. (19-2) and (19-3) into Eq. (23), by using Eq. (24-1), results in

$$D_2=\frac{i(\chi_3-\chi_4)}{\xi(\chi_1\chi_4-\chi_2\chi_3)}\int_{-1}^{1}\phi(\omega,s)\exp(-\mathrm{i}\omega\xi)\mathrm{d}\omega \tag{25}$$

In addition, substituting Eqs. (17), (19-2), (22-2), and (25) into (16-1) leads to the singular integral equation:

$$\begin{aligned}&\int_{-1}^{1}\phi(\omega,s)\left[\frac{1}{\omega-x'}-L(\omega,x',s)\right]\mathrm{d}\omega\\ &\quad=2\pi\left(C_2^{(2)}-C_1^{(2)}\right)\sqrt{\lambda^{(2)}},\quad |x'|<1\end{aligned} \tag{26}$$

where

$$L(\omega,x',s)=\int_0^{\infty}\left[\frac{m^{(2)}(\chi_1-\chi_2)(\chi_3-\chi_4)}{\xi(\chi_1\chi_4-\chi_2\chi_3)}-1\right]\sin[\xi(x'-\omega)]\mathrm{d}\xi \tag{27}$$

The fundamental solution of Eq. (26) is obtained by using Eq. (24-2) as [66]

$$\phi(\omega,s)=\frac{f(\omega,s)}{\sqrt{1-\omega^2}} \tag{28}$$

where $f(\omega,s)$ is Holder-continuous in the domain $-1<\omega<1$. Equations (24-2) and (26) can be solved by the Gauss–Jacobi quadrature method as

$$\sum_{p=1}^{n}\frac{1}{n}f(\omega_p,s)\left[\frac{1}{\omega_p-x_q'}-L\left(\omega_p,x_q',s\right)\right]=4\left(C_2^{(2)}-C_1^{(2)}\right)\sqrt{\lambda^{(2)}} \tag{29-1}$$

$$\sum_{p=1}^{n} f(\omega_p, s) = 0 \tag{29-2}$$

where

$$\omega_p = \cos\left(\frac{2p-1}{2n}\pi\right), \quad p = 1, \ldots, n \tag{30-1}$$

$$x'_q = \cos\left(\frac{q}{n}\pi\right), \quad q = 1, \ldots, n-1 \tag{30-2}$$

Once the function $f(\omega,s)$ is known, $D_2(\xi,s)$ can be obtained by using the Chebyshev–Gauss quadrature method applied to the integral in Eq. (25) as

$$D_2(\xi, s) \approx \frac{\chi_3 - \chi_4}{\xi(\chi_1\chi_4 - \chi_2\chi_3)} \sum_{p=1}^{n} \frac{\pi}{n} f(\omega_p, s) \sin(\omega_p \xi) \tag{31}$$

The temperature field in the Laplace domain can be obtained by substituting Eqs. (22) and (31) into Eq. (19).

The singularity of the heat flux at the crack tip, HFIF, is defined as

$$K_q(t) = \lim_{x \to c} \sqrt{2(x-c)}\, q_y^{(2)}(x, 0, t) \tag{32}$$

By normalizing $K_q(t)$ with $K'_q(t') = K_q(t)\sqrt{c}/(k^{(0)}T_\infty)$, the HFIF in the Laplace domain is obtained as

$$\widetilde{K}'_q(s) = \frac{1}{2}\beta^{(2)} f(1, s) \tag{33}$$

where $f(1,s)$ is calculated by extrapolating the values for $f(\omega_p,s)$.

We recall that the method presented above can handle a series of Fourier and non-Fourier heat conduction problems in homogeneous and heterogeneous media containing a crack and subjected to transient thermal loads. The results that come from solving the equations above are here obtained via a numeric approach [67] that bypasses the complexity of implementing a closed-form Laplace inversion [68–71]. They are presented in the next section for the temperature and HFIF in the time domain.

5. Results and discussion

Heat transfer in a sandwich panel describes the exchange of thermal energy, which depends on the temperature and heat dissipation through its core and faces. Here we focus on the peaks of temperature and the heat flux intensity factor, as they can compromise the heat conduction capacity of the panel if above admissible values. Parameters that impact the panel thermal response include the relative density of the core, the panel geometry, and the position of the crack. To study their role, we examine a heat exchanger with a sandwich layout, entirely made of Copper [72,73] with thermal properties: $c_V = 385$ J/(kg K), $\rho = 8960$ kg/m^3, and $k = 401$ W/(m K). The skins and foam core of the sandwich heat exchanger are made of one material and are perfectly bonded.

5.1. Validation and phase lag effects

In order to validate the accuracy of the developed methodology, non-dimensional temperature time-history of the crack midpoints at the upper and lower surfaces of a cracked half-space is compared in Fig. 2a with those reported in the literature [49]. The homogeneous medium containing a thermally insulated crack parallel to the boundary, $h'_4 = 1$, is subjected to a sudden temperature rise $T'_b = 1$. As a result, the temperature increases to reach its maximum value and then fluctuates to reach the steady state due to thermal energy dissipation. As seen in Fig. 2a, the temperature at the lower midpoint, close to the boundary, is higher than that at the upper midpoint. We recall that the non-zero temperature at the initial stages of the temperature and HFIF time-histories stem from the numerical errors of the numerical Laplace inversion technique used in this paper. The effects of phase-lags on temperature and HFIF histories are also depicted in Fig. 2. As shown in Fig. 2a, increasing the phase-lag of heat flux τ'_q and decreasing the phase-lag of temperature gradient τ'_T could enhance the maximum temperature and shorten the time needed for reaching the maximum temperature. In contrast to the maximum temperature, the maximum HFIF decreases for higher τ'_q and lower τ'_T. These observations are aligned with the results reported in literature [46,47].

5.2. Temporal evolution of temperature and HFIF for given relative densities of the sandwich core

In this section and the followings, non-dimensional phase-lags are assumed as $\tau'_q = 0.5$ and $\tau'_T = 0.2$, with $T'_a = 1$ and $T'_b = 2$ as the non-dimensional temperature at the top and bottom faces of the sandwich. These data are used to visualize the thermal response of a heat exchanger in charts where we span ρ_r from very low density to $\rho_r = 1$.

Fig. 3 illustrates the thermal response of a sandwich panel with geometry: $h'_1 = h'_2 = 0.5$ and $h'_3 = h'_4 = 1$ (Fig. 1). The crack is centered in the panel core with a transient thermal disturbance that is applied on the bottom ($T'_b = 2$) and top of the faces ($T'_a = 1$). Plotted with respect to the relative density (ρ_r) of the foam core, the non-dimensional temperature refers to the temperature at the midpoints of the crack surfaces.

As expected, the first observation that we gather from Fig. 3 is that a reduction in relative density lowers the thermal diffusivity of the foam core, which leads to a decrease in the thermal wave speed. A second insight that we can gain is on the time required for thermal dissipation. Here the key player is the non-dimensional thermal wave speed, $C_{DPL} = \sqrt{2d\tau'_T/(d^{(0)}\tau'^2_q)}$, which is a function of the thermal diffusivity and phase lags of the material constituents of the skin and foam core. This relation explains why a decrease in relative density causes higher amplitude of temperature fluctuation besides greater fluctuation frequency. In addition, as the foam core becomes lighter, the heat flow passing through the core is delayed, thereby increasing the peak of the maximum temperature within the sandwich. For very low values of relative density ($\rho_r \leq 0.07$), however, we note that the maximum temperature at the crack midpoint can have an opposite trend, as shown later in Fig. 6. It is noteworthy that the non-Fourier model presented here allows capturing temperature values exceeding those that can appear at the boundaries of a sandwich panel. This phenomenon of overshooting [74], which cannot be picked up by Fourier heat conduction theory, can cause panel overheating.

Fig. 4 illustrates how the temperature distributes within the sandwich panel for the relative densities examined in Fig. 3. The maps are plotted for temperature values taken at the time the highest temperature occurs.

As we can observe, since a higher change in temperature is applied to the bottom face of the sandwich, the temperature in the lower half of the panel is higher than that of the upper part. The thermal insulation of the crack prevents the heat flow from passing through, which explains why the temperature field is no longer uniform along the x'-direction at each point in the y' direction. The reflection of the heat flow at the crack surfaces causes the magnification of the high temperature at the midpoint of the lower surface of the crack. While a decrease in relative density ρ_r reduces the heat flux, a lower ρ_r could result in a higher rise of temperature within the sandwich panel, a phenomenon that often occurs around the crack midpoint.

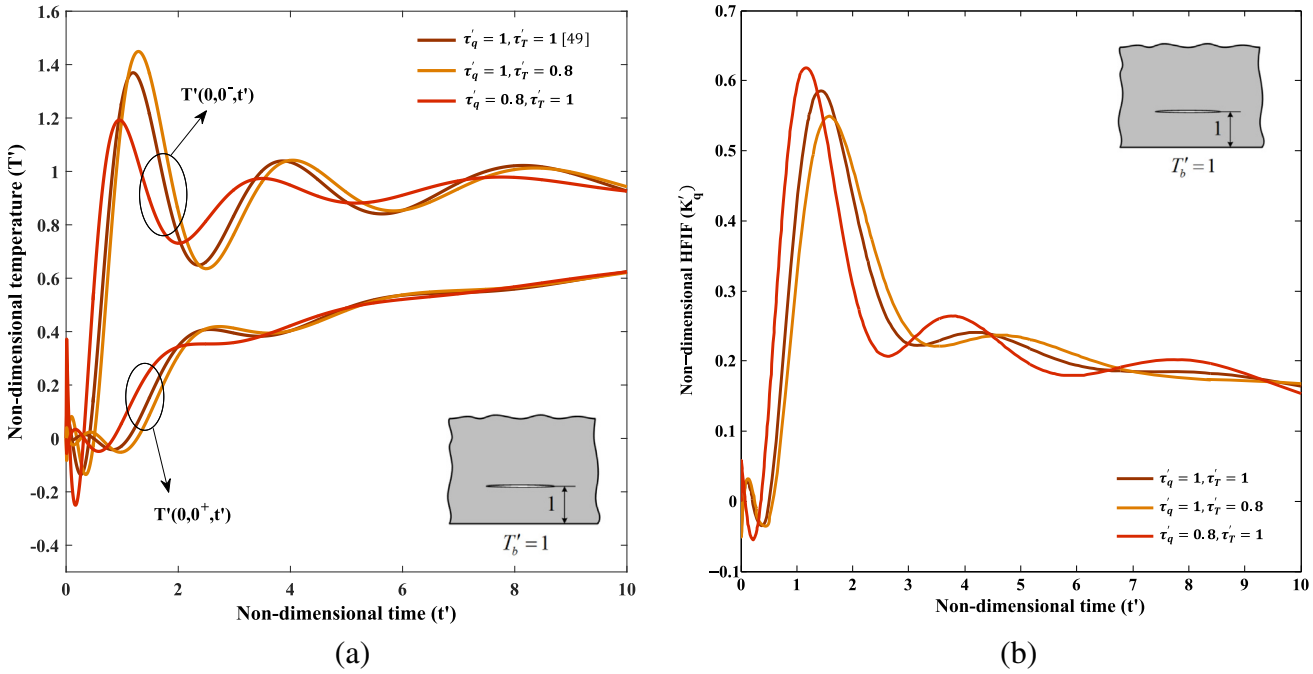

Fig. 2. Effect of phase-lags on non-dimensional transient: (a) temperature at the crack surface midpoints and (b) HFIF.

Finally, the impact of relative density on the transient non-dimensional HFIF is shown in Fig. 5 for the sandwich panel examined in Figs. 3 and 4. The HFIF response domain is depicted for relative densities in the range of $0.01 \leq \rho_r \leq 1$. As expected, the higher the relative density, the greater the maximum and steady-state HFIF.

5.3. Maximum temperature vs. maximum HFIF: the role of relative density and skin thickness

We now use the model presented in Section 4 to apply a sudden temperature rise to the bottom face of a sandwich panel with a crack located in its middle. The overall panel thickness is kept constant,

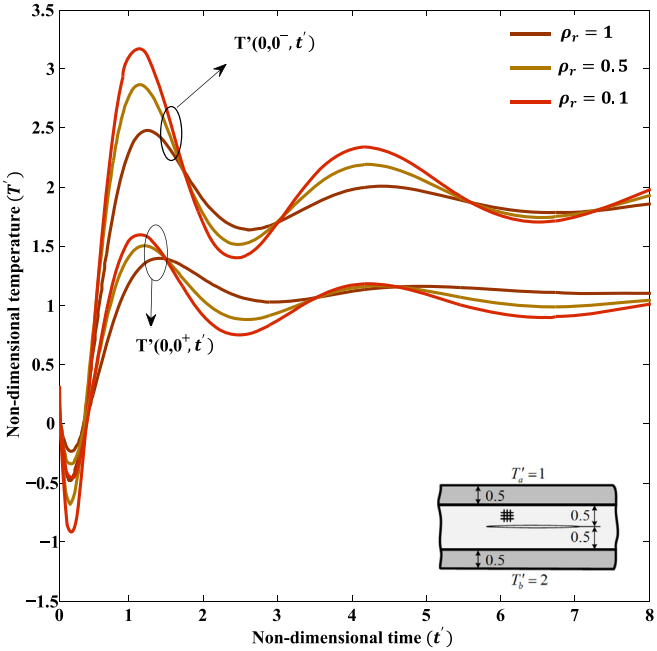

Fig. 3. Temporal evolution of non-dimensional temperature at the crack surface midpoints for three values of relative densities of the core.

whereas the thickness and relative density of the foam core can vary respectively in the range $0.001 \leq h'_1 = h'_2 \leq 1$ and $0.01 \leq \rho_r \leq 1$. From all the values within these ranges, we can obtain the overall thermal response of the panel. This domain of almost triangular shape is shown in Fig. 6. Within it, fall all the intermediate panel configurations with relative density and thickness of the sandwich core limited to the specified ranges. Its bounds are defined by given values of the core thickness (curve ***ad*** on the left for $h'_1 = 1$, and curve ***cd*** on the right for $h'_1 = 0.42$) and of relative density (curve ***ac*** on the bottom for $\rho_r = 0.01$, and the top vertex ***d*** for $\rho_r = 1$).

In Fig. 6 two systems of curves emerge: one with curves almost vertical, e.g. ***ad***, ***cd***, and another one with a rather horizontal path, e.g. ***efgk*** and ***lmn***. The former represents the HFIF and maximum temperature for panel configurations of increasing relative densities, from lightweight to heavy. All converge to point ***d***, a solid material panel. Points on ***ad*** are for a degenerated panel with no skin and made all of foam; heavier foams moving up on ***ad*** make HFIF rise. Similarly, points on ***bd*** describe sandwich panel configurations with prescribed core thickness ($h'_1 = 0.8$), with lower density foams (points close to ***b***) displaying lower HFIF. The second system of curves, e.g. ***efgk*** and ***lmn***, shows thermal response evolutions for panels with varying face thickness and a prescribed relative density of the core.

Whereas higher maximum HFIF are observed in increasingly thicker skins (from ***e*** to ***k*** through ***g***), the maximum temperature at the crack midpoint first is seen to increase for panels from ***e*** to ***g*** ($h'_1 \approx 0.42$) before decreasing again from ***g*** to ***k***. We remark that the final points of the evolution curves, e.g. ***k*** and ***n***, are plotted for a very thin foam core ($h'_1 = 0.001$), for which the three-layer model can still apply. If the core disappears, then the thermal response becomes equal to that of a fully solid panel, point ***d***.

Fig. 6a shows also a dark yellow region, defined by curves ***ae*** and ***bf***, besides ***ab*** and ***ef***. This domain pertains to relatively thin sandwich panels (h'_1 above 0.8) with lightweight core (relative density below 0.3), a quite common range of parameters used in thermal management applications [1,22].

As a counterpart map, Fig. 6b plots evolutions of temperature contours for given core thickness: $h'_1 = 0.5$ and $h'_1 = 0.86$. The

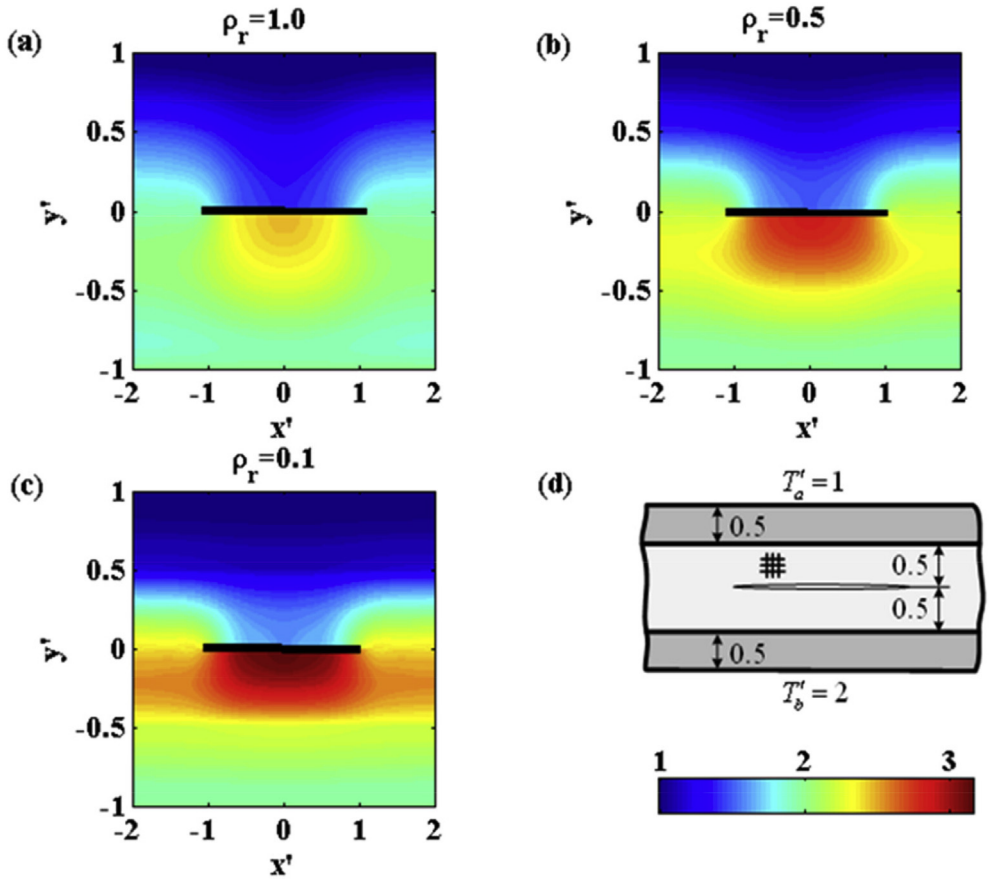

Fig. 4. Non-dimensional temperature distribution of a symmetric cracked sandwich panel for alternative relative densities of the foam core at the time the highest temperature occurs.

latter value of h_1' is chosen, as an example, to represent panels commonly used in aerospace for actively cooled systems with load-bearing capacity [22]. The curves for $h_1' = 0.5$ and $h_1' = 0.86$ reveal how the core thickness could alter the evolution of the temperature contours in a sandwich panel with foam core of alternative densities. The maximum temperature at the midpoint of the crack for a given relative density, is higher for $h_1' = 0.5$ than for $h_1' = 0.86$, as confirmed in Fig. 6a too. While decreasing the relative density of the foam core makes the panel lighter and with superior thermal insulation, the maximum temperature within the sandwich depends on the value of both the relative density (ρ_r) and the thickness ($2h_1'$) of the core. If for $h_1' = 0.5$ we reduce the relative density moving along the ***ABC*** path, the maximum temperature increases from ***A*** ($\rho_r = 1$) to point ***B*** ($\rho_r = 0.07$), as opposed to the trend observed from ***B*** to ***C*** ($\rho_r = 0.01$). Similarly for a sandwich panel with $h_1' = 0.86$, we notice a maximum temperature at point ***D*** for $\rho_r = 0.7$. Furthermore, between A and E ($0.47 \leq \rho_r \leq 1$), the maximum temperature is slightly higher than that of a fully solid panel, A. As seen in Fig. 6, a trade-off between maximum temperature and HFIF could be observed in thermal responses depending on the relative density and thickness of the core.

Fig. 7 illustrates the role of skin thickness and core relative density ($0.01 \leq \rho_r \leq 1$) on the maximum non-dimensional temperature and HFIF. Thermal boundary conditions and overall sandwich geometry do not change from those assumed in Figs. 3–5, except for the skin thickness ($h_c' = h_3' - h_1'$), which varies from 0.01 to 1. For a given relative density of the foam core, Fig. 7a shows the temperature is maximized at optimal skin thickness, e.g. ***A***, ***B***, ***C***, and ***D***. For instance, for a relative density $\rho_r = 0.1$ of the foam, the maximum temperature $T' = 3.18$ occurs for a skin thickness of $h_c' = 0.49$ (point ***A*** in Fig. 7a), which provides safeguard against overheating in thermal management applications. As expected, lighter foam cores experience higher values of maximum temperature. While the maximum temperature for $h_c' = 0.01$ and $\rho_r = 0.1$ is

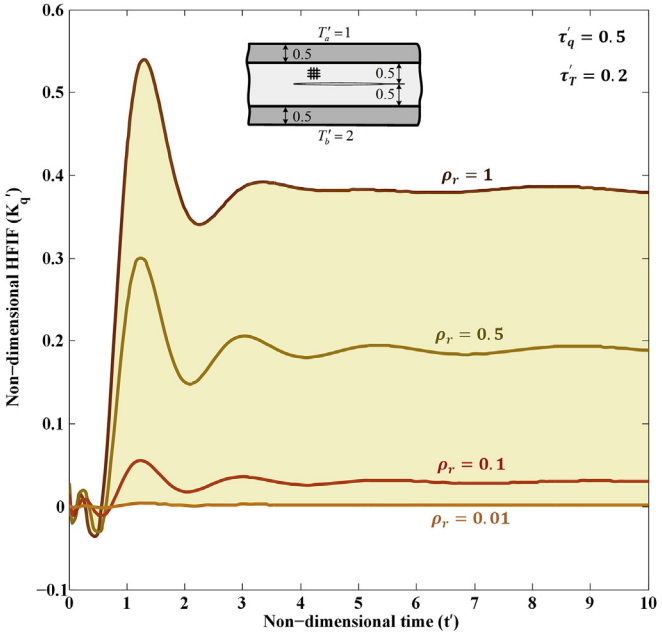

Fig. 5. Non-dimensional transient HFIF of a symmetrically cracked sandwich panel for alternative values of the core relative density.

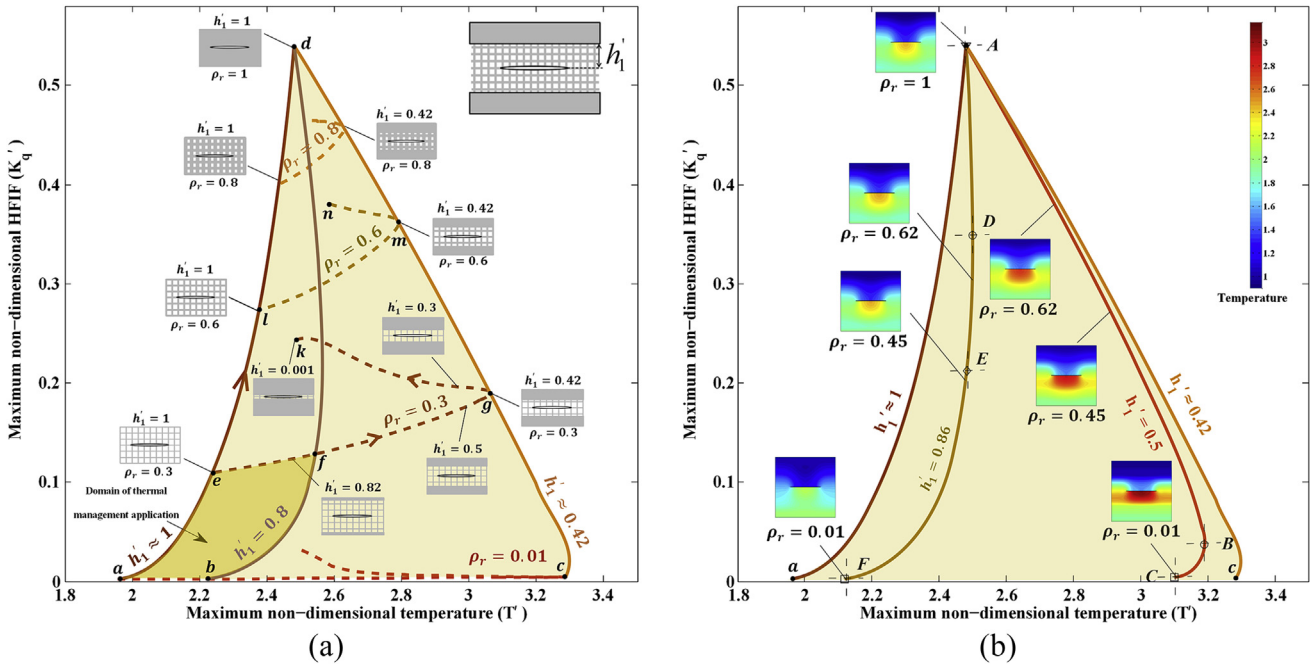

Fig. 6. Design chart of a sandwich panel for maximum non-dimensional temperature at the midpoint of the crack vs. HFIF: (a) evolution responses for the relative density of the core and the skin thickness; (b) temperature contour evolutions. Marked points are: ***A*** ($h_1'=1,\ \rho_r=1$), ***B*** ($h_1'=0.5,\ \rho_r=0.07$), ***C*** ($h_1'=0.5,\ \rho_r=0.01$), ***D*** ($h_1'=0.86,\ \rho_r=0.7$), ***E*** ($h_1'=0.86,\ \rho_r=0.47$), and ***F*** ($h_1'=0.86,\ \rho_r=0.01$).

6.0% higher than that of a solid core ($\rho_r=1$), for $h_c'=1$ the increase could be up to 38.1%. Fig. 7b shows how the maximum non-dimensional HFIF changes with the skin thickness. While for a solid panel ($\rho_r=1$), the maximum HFIF decreases for higher h_c', no pronounced variation is observed for a lighter core.

5.4. Maximum temperature vs. maximum HFIF: the role of crack location and relative density

Fig. 8 shows the impact of crack position on the maximum non-dimensional temperature and HFIF, for given core and skin thickness ($h_1'+h_2'=1,\ h_3'=h_4'=1$) and a range of relative density ($0.01\le\rho_r\le 1$). The maximum temperature and maximum HFIF vary nonlinearly as the crack moves from the top face towards the bottom face of the foam core. The optimum values of the temperature (global maximum) and HFIF (global minimum) are marked in Fig. 8 with capital (***A***, ***B***, ***C***, and ***D***) and small (***a***, ***b***, ***c***, and ***d***) letters, respectively. The optimum values occur where the crack is located around the center of the panel; for $\rho_r=0.1$, the optimum maximum temperature ($T'=3.24$) and maximum HFIF ($K_q'=0.054$) occur, respectively, at point ***D*** with $h_1'=0.57$ and point ***d*** with $h_1'=0.47$. The maximum temperature and maximum HFIF within a sandwich panel with a crack close to the lower skin are higher than that with a crack close to the upper skin. For example for $\rho_r=0.3$, by varying

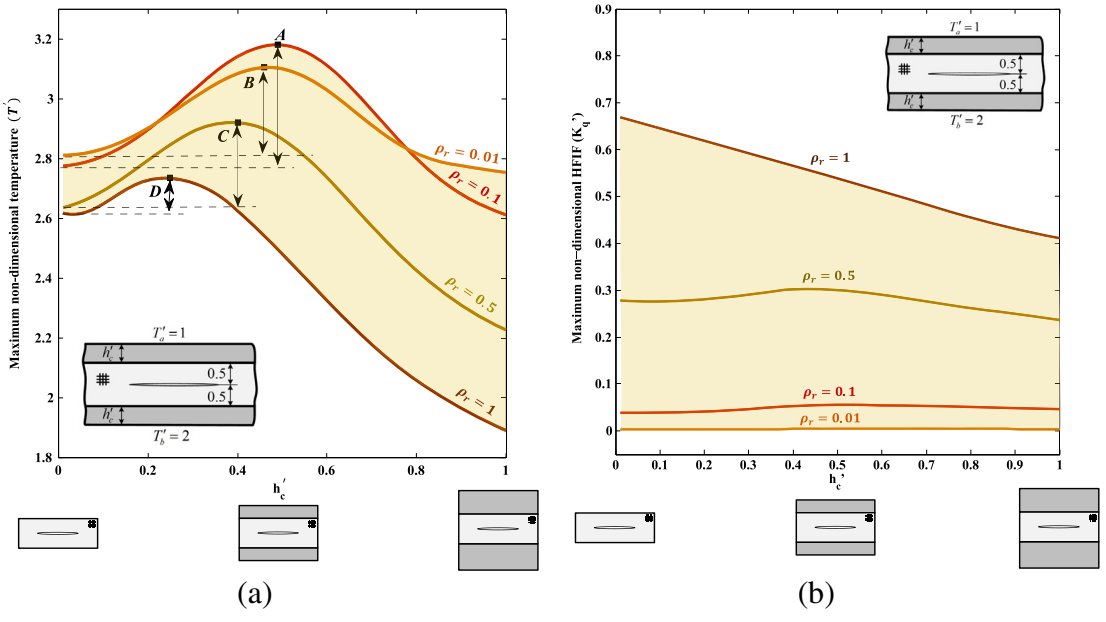

Fig. 7. Effect of skin thickness on maximum non-dimensional (a) temperature and (b) HFIF for a symmetrically cracked panel of given relative densities. Marked points are: ***A*** ($\rho_r=0.1,\ h_c'=0.49$), ***B*** ($\rho_r=0.01,\ h_c'=0.46$), ***C*** ($\rho_r=0.5,\ h_c'=0.4$), and ***D*** ($\rho_r=1,\ h_c'=0.25$).

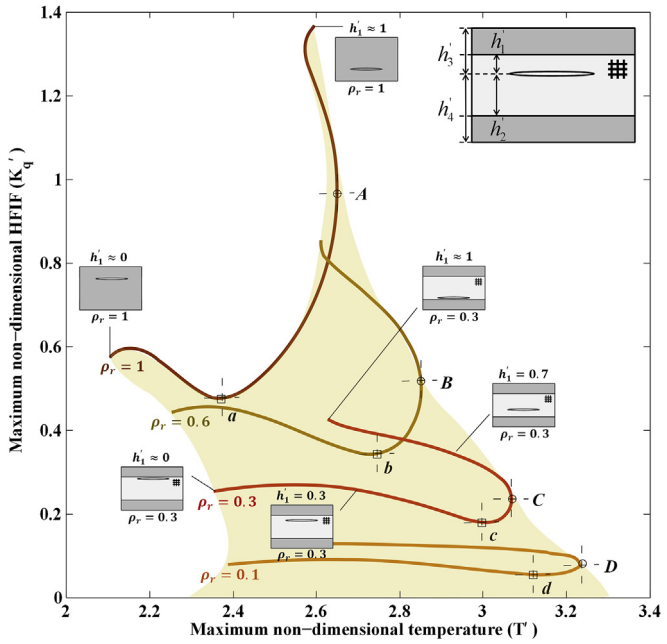

Fig. 8. Effect of crack position on maximum non-dimensional temperature at the crack midpoint and HFIF for an asymmetrically cracked sandwich panel. Marked points are: ***A*** ($\rho_r = 1, h_1' = 0.75$), ***a*** ($\rho_r = 1, h_{1a}' = 0.4$), ***B*** ($\rho_r = 0.6, h_1' = 0.64$), ***b*** ($\rho_r = 0.6, h_1' = 0.47$), ***C*** ($\rho_r = 0.3, h_1' = 0.57$), ***c*** ($\rho_r = 0.3, h_1' = 0.47$), ***D*** ($\rho_r = 0.1, h_1' = 0.57$), ***d*** ($\rho_r = 0.1, h_1' = 0.47$).

the crack position from $h_1' = 0.01$ to $h_1' = 0.99$ the maximum temperature and maximum HFIF increase by 11.6% and 68.3%. The response domain given in Fig. 8 covers the whole range of crack positions and can thus be used to determine the safety factor for thermal design.

6. Concluding remarks

This paper has presented an investigation on non-Fourier heat conduction in a sandwich panel with a crack in the core parallel to the panel faces, upon which the temperature has been suddenly raised. The transient temperature field and heat flux intensity factor have been obtained by Laplace and Fourier integral transforms. The role of phase-lags, relative density, and thickness of the core, besides skin thickness and crack position, has been studied with results visualized in maps of thermal responses. We have found that the increase of the phase-lag of the heat flux and the decrease of the phase-lag of the temperature gradient, on one hand, enhance the maximum temperature, and on the other hand, reduce the maximum HFIF. Although decreasing the relative density of the foam core reduces the thermal wave speed, its effect on the maximum temperature and HFIF can be in conflict for given geometries of the skin and foam core, as well as for certain positions of the crack in the core. For instance, while the weight and heat flux intensity factor for a cellular core of $\rho_r = 0.05$ are 48% and 95% lower than those for a solid core, the maximum temperature of the panel is 28% higher than that for a solid panel. The method and charts provided in this paper contribute to elucidate the role that the geometric parameters defining the skin and core of a sandwich panel paly in thermal management applications where the sandwich panel is used for example as a heat exchanger. The methodology can be extended to analyze thermal stresses in cracked and deboned sandwich panels and to understand the effect of crack propagation in a thermally insulated domain.

Acknowledgments

A.H. Akbarzadeh acknowledges financial supports by Natural Sciences and Engineering Research Council of Canada (NSERC).

Appendix

Non-zero components of **A** and **E** in Eq. (20) are given as

$$A_{11} = T_a'/s, \quad A_{21} = T_b'/s, \tag{A.1}$$

$$E_{11} = \exp\left(\sqrt{\lambda^{(1)}}h_3'\right), \quad E_{12} = \exp\left(-\sqrt{\lambda^{(1)}}h_3'\right), \quad E_{25} = \exp\left(-\sqrt{\lambda^{(3)}}h_4'\right)$$

$$E_{26} = \exp\left(\sqrt{\lambda^{(3)}}h_4'\right), \quad E_{31} = \exp\left(\sqrt{\lambda^{(1)}}h_1'\right), \quad E_{32} = -\exp\left(-\sqrt{\lambda^{(1)}}h_1'\right)$$

$$E_{33} = -\frac{\beta^{(2)}}{\beta^{(1)}}\frac{\sqrt{\lambda^{(2)}}}{\sqrt{\lambda^{(1)}}}\exp\left(\sqrt{\lambda^{(2)}}h_1'\right), \quad E_{34} = \frac{\beta^{(2)}}{\beta^{(1)}}\frac{\sqrt{\lambda^{(2)}}}{\sqrt{\lambda^{(1)}}}\exp\left(-\sqrt{\lambda^{(2)}}h_1'\right)$$

$$E_{41} = \left(1-\beta^{(1)}X_1\sqrt{\lambda^{(1)}}\right)\exp\left(\sqrt{\lambda^{(1)}}h_1'\right), \quad E_{42} = \left(1+\beta^{(1)}X_1\sqrt{\lambda^{(1)}}\right)\exp\left(-\sqrt{\lambda^{(1)}}h_1'\right)$$

$$E_{43} = -\exp\left(\sqrt{\lambda^{(2)}}h_1'\right), \quad E_{44} = -\exp\left(-\sqrt{\lambda^{(2)}}h_1'\right) \tag{A.2}$$

$$E_{53} = \exp\left(-\sqrt{\lambda^{(2)}}h_2'\right), \quad E_{54} = -\exp\left(\sqrt{\lambda^{(2)}}h_2'\right)$$

$$E_{55} = -\frac{\beta^{(3)}}{\beta^{(2)}}\frac{\sqrt{\lambda^{(3)}}}{\sqrt{\lambda^{(2)}}}\exp\left(-\sqrt{\lambda^{(3)}}h_2'\right), \quad E_{56} = \frac{\beta^{(3)}}{\beta^{(2)}}\frac{\sqrt{\lambda^{(3)}}}{\sqrt{\lambda^{(2)}}}\exp\left(\sqrt{\lambda^{(3)}}h_2'\right)$$

$$E_{63} = \exp\left(-\sqrt{\lambda^{(2)}}h_2'\right), \quad E_{64} = \exp\left(\sqrt{\lambda^{(2)}}h_2'\right)$$

$$E_{65} = -\left(1+\beta^{(3)}X_2\sqrt{\lambda^{(3)}}\right)\exp\left(-\sqrt{\lambda^{(3)}}h_2'\right), \quad E_{66} = -\left(1-\beta^{(3)}X_2\sqrt{\lambda^{(3)}}\right)\exp\left(\sqrt{\lambda^{(3)}}h_2'\right)$$

and the coefficients introduced in Eq. (22) are defined as

$$\begin{aligned}
\chi_1 &= \left(1+\beta^{(1)}X_1m^{(1)}-\frac{\beta^{(1)}m^{(1)}}{\beta^{(2)}m^{(2)}}\right)\exp\left(-m^{(2)}h_1'-m^{(1)}h_1'\right)-\left(1-\beta^{(1)}X_1m^{(1)}+\frac{\beta^{(1)}m^{(1)}}{\beta^{(2)}m^{(2)}}\right)\exp\left(m^{(1)}h_1'-2m^{(1)}h_3'-m^{(2)}h_1'\right)\\
\chi_2 &= \left(1+\beta^{(1)}X_1m^{(1)}+\frac{\beta^{(1)}m^{(1)}}{\beta^{(2)}m^{(2)}}\right)\exp\left(m^{(2)}h_1'-m^{(1)}h_1'\right)-\left(1-\beta^{(1)}X_1m^{(1)}-\frac{\beta^{(1)}m^{(1)}}{\beta^{(2)}m^{(2)}}\right)\exp\left(m^{(1)}h_1'-2m^{(1)}h_3'+m^{(2)}h_1'\right)\\
\chi_3 &= \left(1+\beta^{(3)}X_2m^{(3)}+\frac{\beta^{(3)}m^{(3)}}{\beta^{(2)}m^{(2)}}\right)\exp\left(m^{(2)}h_2'-m^{(3)}h_2'\right)-\left(1-\beta^{(3)}X_2m^{(3)}-\frac{\beta^{(3)}m^{(3)}}{\beta^{(2)}m^{(2)}}\right)\exp\left(m^{(3)}h_2'-2m^{(3)}h_4'+m^{(2)}h_2'\right)\\
\chi_4 &= \left(1+\beta^{(3)}X_2m^{(3)}-\frac{\beta^{(3)}m^{(3)}}{\beta^{(2)}m^{(2)}}\right)\exp\left(-m^{(2)}h'-m^{(3)}h_2'\right)-\left(1-\beta^{(3)}X_2m^{(3)}-\frac{\beta^{(3)}m^{(3)}}{\beta^{(2)}m^{(2)}}\right)\exp\left(m^{(3)}h_2'-2m^{(3)}h_4'-m^{(2)}h_2'\right)
\end{aligned} \tag{A.3}$$

References

[1] L.J. Gibson, M.F. Ashby, Cellular Solids: Structure and Properties, Cambridge University Press, 1997.
[2] M.F. Ashby, D. Cebon, Materials selection in mechanical design, J. Phys. IV 3 (C7) (1993). C7-1–C7-9.
[3] H.N. Wadley, N.A. Fleck, A.G. Evans, Fabrication and structural performance of periodic cellular metal sandwich structures, Compos. Sci. Technol. 63 (16) (2003) 2331–2343.
[4] H.N. Wadley, Multifunctional periodic cellular metals, Philos. Trans. R. Soc. Lond. A Math. Phys. Eng. Sci. 364 (1838) (2006) 31–68.
[5] A.H. Akbarzadeh, D. Pasini, Phase-lag heat conduction in multilayered cellular media with imperfect bonds, Int. J. Heat Mass Transfer 75 (2014) 656–667.
[6] V.J. Challis, et al., Computationally generated cross-property bounds for stiffness and fluid permeability using topology optimization, Int. J. Solids Struct. 49 (23) (2012) 3397–3408.
[7] J.K. Guest, J.H. Prévost, Optimizing multifunctional materials: design of microstructures for maximized stiffness and fluid permeability, Int. J. Solids Struct. 43 (22) (2006) 7028–7047.
[8] S. Torquato, et al., Effective mechanical and transport properties of cellular solids, Int. J. Mech. Sci. 40 (1) (1998) 71–82.
[9] J. Huang, J. Lin, Mixed-mode fracture of brittle cellular materials, J. Mater. Sci. 31 (10) (1996) 2647–2652.
[10] A. Rafsanjani, A.H. Akbarzadeh, D. Pasini, Snapping mechanical metamaterials under tension, Adv. Mater. 27 (39) (2015) 5931–5935.
[11] M.S. Elsayed, D. Pasini, Multiscale structural design of columns made of regular octet-truss lattice material, Int. J. Solids Struct. 47 (14) (2010) 1764–1774.
[12] A. Vigliotti, D. Pasini, Mechanical properties of hierarchical lattices, Mech. Mater. 62 (2013) 32–43.
[13] E.M.K. Abad, S.A. Khanoki, D. Pasini, Fatigue design of lattice materials via computational mechanics: application to lattices with smooth transitions in cell geometry, Int. J. Fatigue 47 (2013) 126–136.
[14] S. Arabnejad, D. Pasini, Mechanical properties of lattice materials via asymptotic homogenization and comparison with alternative homogenization methods, Int. J. Mech. Sci. 77 (2013) 249–262.
[15] A.H. Akbarzadeh, et al., Dynamic eigenstrain behavior of magnetoelastic functionally graded cellular cylinders, Compos. Struct. 116 (2014) 404–413.
[16] O. Kesler, L. Gibson, Size effects in metallic foam core sandwich beams, Mater. Sci. Eng. A 326 (2) (2002) 228–234.
[17] V. Tagarielli, V. Deshpande, N. Fleck, The dynamic response of composite sandwich beams to transverse impact, Int. J. Solids Struct. 44 (7) (2007) 2442–2457.
[18] D.T. Queheillalt, et al., A multifunctional heat pipe sandwich panel structure, Int. J. Heat Mass Transfer 51 (1) (2008) 312–326.
[19] E. Sadeghi, S. Hsieh, M. Bahrami, Thermal conductivity and contact resistance of metal foams, J. Phys. D Appl. Phys. 44 (12) (2011) 125406.
[20] K.J. Maloney, et al., Multifunctional heat exchangers derived from three-dimensional micro-lattice structures, Int. J. Heat Mass Transfer 55 (9) (2012) 2486–2493.
[21] J.F. Rakow, A.M. Waas, Thermal buckling of metal foam sandwich panels for convective thermal protection systems, J. Spacecraft Rockets 42 (5) (2005) 832–844.
[22] J.F. Rakow, A.M. Waas, Response of actively cooled metal foam sandwich panels exposed to thermal loading, AIAA J. 45 (2) (2007) 329–336.
[23] L.R. Xu, A.J. Rosakis, Impact failure characteristics in sandwich structures: part I: basic failure mode selection, Int. J. Solids Struct. 39 (16) (2002) 4215–4235.
[24] S. Choi, B.V. Sankar, A micromechanical method to predict the fracture toughness of cellular materials, Int. J. Solids Struct. 42 (5) (2005) 1797–1817.
[25] S.-J. Lee, J. Wang, B.V. Sankar, A micromechanical model for predicting the fracture toughness of functionally graded foams, Int. J. Solids Struct. 44 (11) (2007) 4053–4067.
[26] F. Lipperman, M. Ryvkin, M.B. Fuchs, Nucleation of cracks in two-dimensional periodic cellular materials, Comput. Mech. 39 (2) (2007) 127–139.
[27] A. Leach, The thermal conductivity of foams. I. Models for heat conduction, J. Phys. D Appl. Phys. 26 (5) (1993) 733.
[28] T. Lu, H. Stone, M. Ashby, Heat transfer in open-cell metal foams, Acta Mater. 46 (10) (1998) 3619–3635.
[29] J. Tian, et al., The effects of topology upon fluid-flow and heat-transfer within cellular copper structures, Int. J. Heat Mass Transfer 47 (14) (2004) 3171–3186.
[30] G. Sih, Heat conduction in the infinite medium with lines of discontinuities, J. Heat Transfer 87 (2) (1965) 293–298.
[31] T. Da Yu, The singular behavior of the temperature gradient in the vicinity of a macrocrack tip, Int. J. Heat Mass transfer 33 (12) (1990) 2625–2630.
[32] D. Tzou, The effect of thermal conductivity on the singular behavior of the near-tip temperature gradient, J. Heat Transfer 113 (4) (1991) 806–813.
[33] T.-C. Chiu, S.-W. Tsai, C.-H. Chue, Heat conduction in a functionally graded medium with an arbitrarily oriented crack, Int. J. Heat Mass Transfer 67 (2013) 514–522.
[34] C.K. Chao, L.Y. Kuo, Thermal problem of curvilinear cracks in bonded dissimilar materials with a point heat source, Int. J. Heat Mass Transfer 36 (17) (1993) 4085–4093.
[35] T. Lu, N. Fleck, The thermal shock resistance of solids, Acta Mater. 46 (13) (1998) 4755–4768.
[36] L. Zhao, T. Lu, N. Fleck, Crack channelling and spalling in a plate due to thermal shock loading, J. Mech. Phys. Solids 48 (5) (2000) 867–897.
[37] A.H. Akbarzadeh, M. Babaei, Z. Chen, Thermopiezoelectric analysis of a functionally graded piezoelectric medium, Int. J. Appl. Mech. 3 (01) (2011) 47–68.
[38] A.H. Akbarzadeh, M. Babaei, Z. Chen, Coupled thermopiezoelectric behaviour of a one-dimensional functionally graded piezoelectric medium based on C–T theory, Proc. Inst. Mech. Eng. C. J. Mech. Eng. Sci. 225 (11) (2011) 2537–2551.
[39] D.S. Chandrasekharaiah, Hyperbolic thermoelasticity: a review of recent literature, Appl. Mech. Rev. 51 (12) (1998) 705–729.
[40] C. Korner, H.W. Bergmann, The physical defects of the hyperbolic heat conduction equation, Appl. Phys. A. Mater. Sci. Process. 67 (4) (1998) 397–401.
[41] D. Tzou, A unified field approach for heat conduction from macro-to micro-scales, J. Heat Transfer 117 (1) (1995) 8–16.
[42] K.-C. Liu, Analysis of dual-phase-lag thermal behaviour in layered films with temperature-dependent interface thermal resistance, J. Phys. D: Appl. Phys. 38 (19) (2005) 3722.
[43] K. Ramadan, Treatment of the interfacial temperature jump condition with non-Fourier heat conduction effects, Int. Commun. Heat Mass Transfer 35 (9) (2008) 1177–1182.
[44] Y. Zhang, Generalized dual-phase lag bioheat equations based on nonequilibrium heat transfer in living biological tissues, Int. J. Heat Mass Transfer 52 (21) (2009) 4829–4834.
[45] A.H. Akbarzadeh, Z.T. Chen, Transient heat conduction in a functionally graded cylindrical panel based on the dual phase lag theory, Int. J. Thermophys. 33 (6) (2012) 1100–1125.
[46] A.H. Akbarzadeh, Z.T. Chen, Heat conduction in one-dimensional functionally graded media based on the dual-phase-lag theory, Proc. Inst. Mech. Eng., C: J. Mech. Eng. Sci. 227 (4) (2013) 744–759.

[47] A.H. Akbarzadeh, J.W. Fu, Z.T. Chen, Three-phase-lag heat conduction in a functionally graded hollow cylinder, Trans. Can. Soc. Mech. Eng. 38 (1) (2014) 155–171.
[48] A.H. Akbarzadeh, Z.T. Chen, Dual phase lag heat conduction in functionally graded hollow spheres, Int. J. Appl. Mech. 6 (2014) 1450002 (27 p.).
[49] K. Hu, Z. Chen, Transient heat conduction analysis of a cracked half-plane using dual-phase-lag theory, Int. J. Heat Mass Transfer 62 (2013) 445–451.
[50] B. Wang, J. Han, Non-Fourier heat conduction in layered composite materials with an interface crack, Int. J. Eng. Sci. 55 (2012) 66–75.
[51] J. Fu, et al., Non-Fourier thermoelastic behavior of a hollow cylinder with an embedded or edge circumferential crack, Eng. Fract. Mech. 128 (2014) 103–120.
[52] D. Pasini, Shape and material selection for optimizing flexural vibrations in multilayered resonators, Microelectromech. Syst. J. 15 (6) (2006) 1745–1758.
[53] D. Pasini, Shape transformers for material and shape selection of lightweight beams, Mater. Des. 28 (7) (2007) 2071–2079.
[54] D. Pasini, Bend stiffness of laminate microstructures containing three dissimilar materials, Int. J. Mech. Mater. Des. 5 (2) (2009) 175–193.
[55] K. Hu, Z. Chen, Thermoelastic analysis of a partially insulated crack in a strip under thermal impact loading using the hyperbolic heat conduction theory, Int. J. Eng. Sci. 51 (2012) 144–160.
[56] A.-J. Wang, D. McDowell, In-plane stiffness and yield strength of periodic metal honeycombs, J. Eng. Mater. Technol. 126 (2) (2004) 137–156.
[57] M.F. Ashby, Materials Selection in Mechanical Design, fourth ed., Butterworth-Heinemann, , Amsterdam, 2011.
[58] S.J. Hollister, N. Kikuchi, A comparison of homogenization and standard mechanics analyses for periodic porous composites, Comput. Mech. 10 (2) (1992) 73–95.
[59] D.A. Nield, A. Bejan, Convection in Porous Media, Springer, 2006.
[60] A.H. Akbarzadeh, D. Pasini, Phase-lag heat conduction in multilayered cellular media with imperfect bonds, Int. J. Heat Mass Transfer 75 (2014) 656–667.
[61] M. Ashby, The properties of foams and lattices, Philos. Trans. R. Soc. Lond. A: Math. Phys. Eng. Sci. 364 (1838) (2006) 15–30.
[62] L. Debnath, D. Bhatta, Integral Transforms and Their Applications, CRC Press, 2010.
[63] J.W. Fu, Z.T. Chen, L.F. Qian, Coupled thermoelastic analysis of a multi-layered hollow cylinder based on the C–T theory and its application on functionally graded materials, Compos. Struct. 131 (2015) 139–150.
[64] J. Zhi-He, N. Naotake, Transient thermal stress intensity factors for a crack in a semi-infinite plate of a functionally gradient material, Int. J. Solids Struct. 31 (2) (1994) 203–218.
[65] N. Noda, J. Zhi-He, Thermal stress intensity factors for a crack in a strip of a functionally gradient material, Int. J. Solids Struct. 30 (8) (1993) 1039–1056.
[66] F. Erdogan, et al., Numerical solution of singular integral equations, in: Methods of Analysis and Solutions of Crack Problems, Springer, 1973, pp. 368–425.
[67] M.K. Miller, W.T.J. Guy, Numerical inversion of the Laplace transform by use of Jacobi polynomials, SIAM J. Numer. Anal. 3 (4) (1966) 624–635.
[68] A.H. Akbarzadeh, M. Abbasi, M. Eslami, Coupled thermoelasticity of functionally graded plates based on the third-order shear deformation theory, Thin-Walled Struct. 53 (2012) 141–155.
[69] A.H. Akbarzadeh, et al., Mechanical behaviour of functionally graded plates under static and dynamic loading, Proc. Inst. Mech. Eng. C: J. Mech. Eng. Sci. 225 (2) (2011) 326–333.
[70] A.H. Akbarzadeh, M. Abbasi, M. Eslami, Dynamic analysis of functionally graded plates using the hybrid Fourier–Laplace transform under thermo-mechanical loading, Meccanica 46 (6) (2011) 1373–1392.
[71] Y. Kiani, et al., Static and dynamic analysis of an FGM doubly curved panel resting on the Pasternak-type elastic foundation, Compos. Struct. 94 (8) (2012) 2474–2484.
[72] N. Tsolas, S. Chandra, Forced convection heat transfer in spray formed copper and nickel foam heat exchanger tubes, J. Heat Transfer 134 (6) (2012) 062602.
[73] K. Boomsma, D. Poulikakos, F. Zwick, Metal foams as compact high performance heat exchangers, Mech. Mater. 35 (12) (2003) 1161–1176.
[74] M. Xu, et al., Thermal wave interference as the origin of the overshooting phenomenon in dual-phase-lagging heat conduction, Int. J. Therm. Sci. 50 (5) (2011) 825–830.